Available online at www.sciencedirect.com
ScienceDirect
Atmospheric Environment 41 (2007) 7588–7602
ATMOSPHERIC ENVIRONMENT
www.elsevier.com/locate/atmosenv

Atmospheric oxalic acid and SOA production from glyoxal: Results of aqueous photooxidation experiments

Annmarie G. Carlton[a], Barbara J. Turpin[b,*], Katye E. Altieri[c], Sybil Seitzinger[c], Adam Reff[d], Ho-Jin Lim[e], Barbara Ervens[f]

[a]*ASMD, ARL, NOAA, Mail Drop E-243-01, Research Triangle Park, NC 27711, USA*
[b]*Department of Environmental Sciences, Rutgers University, 14 College Farm Road, New Brunswick, NJ 08901, USA*
[c]*Institute of Marine and Coastal Sciences, Rutgers University, Rutgers/NOAA CMER Program, 71 Dudley Road, New Brunswick, NJ 08901, USA*
[d]*AMD, NERL, US Environmental Protection Agency, Research Triangle Park, NC 27711, USA*
[e]*Department of Environmental Engineering, Kyungpook National University, Daegu 702-701, Republic of Korea*
[f]*Department of Atmospheric Science, Colorado State University, Fort Collins, CO 80523, USA*

Received 12 February 2007; received in revised form 3 May 2007; accepted 16 May 2007

Abstract

Aqueous-phase photooxidation of glyoxal, a ubiquitous water-soluble gas-phase oxidation product of many compounds, is a potentially important global and regional source of oxalic acid and secondary organic aerosol (SOA). Reaction kinetics and product analysis are needed to validate and refine current aqueous-phase mechanisms to facilitate prediction of in-cloud oxalic acid and SOA formation from glyoxal. In this work, aqueous-phase photochemical reactions of glyoxal and hydrogen peroxide were conducted at pH values typical of clouds and fogs (i.e., pH = 4–5). Experimental time series concentrations were compared to values obtained using a published kinetic model and reaction rate constants from the literature. Experimental results demonstrate the formation of oxalic acid, as predicted by the published aqueous phase mechanism. However, the published mechanism did not reproduce the glyoxylic and oxalic acid concentration dynamics. Formic acid and larger multifunctional compounds, which were not previously predicted, were also formed. An expanded aqueous-phase oxidation mechanism for glyoxal is proposed that reasonably explains the concentration dynamics of formic and oxalic acids and includes larger multifunctional compounds. The coefficient of determination for oxalic acid prediction was improved from 0.001 to >0.8 using the expanded mechanism. The model predicts that less than 1% of oxalic acid is formed through the glyoxylic acid pathway. This work supports the hypothesis that SOA forms through cloud processing of glyoxal and other water-soluble products of alkenes and aromatics of anthropogenic, biogenic and marine origin and provides reaction kinetics needed for oxalic acid prediction.

Keywords: Secondary organic aerosol; Aqueous-phase atmospheric chemistry; Glyoxal; Oxalic acid; Organic PM; Cloud processing

1. Introduction

The generally poor understanding of the sources and formation of secondary organic particulate matter (PM) is a major source of uncertainty in

*Corresponding author. Tel.: +1 732 932 9800x6219; fax: +1 732 932 8644.
E-mail address: turpin@envsci.rutgers.edu (B.J. Turpin).

1352-2310/$ - see front matter © 2007 Elsevier Ltd. All rights reserved.
doi:10.1016/j.atmosenv.2007.05.035

predictions of aerosol concentrations and properties that affect health, visibility and climate (EPA, 2004; IPCC, 2001; Kanakidou et al., 2005). There is growing evidence suggesting that, like sulfate, secondary organic aerosol (SOA) is formed through aqueous-phase reactions in clouds, fogs and aerosols (Blando and Turpin, 2000; Warneck, 2003; Ervens et al., 2004; Crahan et al., 2004; Gelencser and Varga, 2005; Lim et al., 2005; Carlton et al., 2006; Altieri et al., 2006). However, this formation pathway is poorly understood. As was the case for sulfate, model simulation is needed to evaluate the regional and global importance of SOA formed as a result of aqueous-phase atmospheric chemistry. This effort is hampered by the lack of kinetic data for recognized pathways and because many products and pathways are unknown.

A large gap between measurements and model predictions of organic PM was recently observed in the free troposphere (Heald et al., 2005). This discrepancy might arise from atmospheric processes not yet parameterized in current models, such as in-cloud SOA formation. In-cloud SOA formation is likely to enhance organic PM concentrations in the free troposphere and organic aerosol concentrations in locations affected by regional pollutant transport. Predictions and experiments provide strong support for the following. Alkene and aromatic emissions are oxidized in the interstitial spaces of clouds; the water-soluble products partition into cloud droplets, where they oxidize further forming low volatility compounds that remain at least in part in the particle phase after droplet evaporation, forming SOA (Blando and Turpin, 2000; Warneck, 2003; Ervens et al., 2004; Crahan et al., 2004; Gelencser and Varga, 2005; Lim et al., 2005; Carlton et al., 2006; Altieri et al., 2006). Recent kinetic modeling supports in-cloud oxalic acid and thus SOA formation from glyoxal (GLY) and other gas-phase precursors (Warneck, 2003; Ervens et al., 2004; Lim et al., 2005). Measured atmospheric concentration dynamics suggest that GLY is an in-cloud precursor for carboxylic acids (Chebbi and Carlier, 1996) that likely contribute to SOA due to their low volatility (e.g., glyoxylic and oxalic acids). Batch photochemical experiments support the in-cloud SOA hypothesis through product analysis that demonstrates low volatility product formation from GLY (e.g., glyoxylic acid, Buxton et al., 1997) and pyruvic acid (e.g., glyoxylic and oxalic acids, Carlton et al., 2006, and larger oligomeric compounds, Altieri et al., 2006; Guzman et al., 2006) at pH values typical of clouds. Differences between aqueous- and gas-phase chemistry suggest that SOA formation from aldehydes is more favorable in the aqueous phase than in the gas phase. The aqueous medium enables formation of new structures (i.e., gem diols) whose functional groups are oxidized during reactions with $^{\bullet}OH$ and other oxidants, while the C–C bond structure is initially preserved. In contrast, in the gas phase, C–C bonds are usually broken yielding smaller, more volatile compounds (e.g., GLY oxidizes to form volatile compounds, HO_2, CO, HCHO, in the gas phase; Atkinson et al., 2006).

GLY is the gas-phase oxidation product of many compounds of anthropogenic (Kleindienst et al., 1999; Atkinson, 2000; Volkamer et al., 2001; Magneron et al., 2005; Volkamer et al., 2005), biogenic (Atkinson, 2000; Spaulding et al., 2003), and marine (Miller and Moran, 1997; Warneck, 2003) origin. It is found widely in the environment in the gas and aerosol phases and in cloud, fog and dew water (Sempere and Kawamura, 1994; Matsumoto et al., 2005). While GLY is present at concentrations (5–280 μM in cloud water; Munger et al., 1990) lower than SO_2, at cloud relevant pH the water solubility of GLY (effective Henry's law constant, $H_{eff} > 3 \times 10^5\,M\,atm^{-1}$ at 25 °C; Betterton and Hoffmann, 1988) is 3 orders of magnitude greater than that of SO_2. (Cloud processing is an important pathway for particulate sulfate formation from SO_2; Seinfeld and Pandis, 1998.) Also, GLY has fast uptake by droplets (Schweitzer et al., 1998), is observed in cloud water, and is highly reactive in the aqueous phase (Buxton et al., 1997). Therefore, since GLY is ubiquitous in the environment, can enter a cloud or fog droplet readily, and is predicted to form low volatility compounds through aqueous-phase photooxidation, SOA formation through cloud processing of GLY is likely. It is important to note that low volatility products (e.g., glyoxylic and oxalic acids) are expected from aqueous-phase GLY oxidation but gas-phase oxidation produces high volatility compounds (e.g., HO_2, CO, HCHO) not expected to contribute to SOA directly (Ervens et al., 2004). Other similar water-soluble organics are found in clouds (Kawamura et al., 1996a, b) and are likely to contribute to in-cloud SOA formation as well (e.g., methylglyoxal and glycolaldehyde; Warneck, 2003; Ervens et al., 2004; Lim et al., 2005).

Dicarboxylic acids are similarly ubiquitous in the atmosphere and oxalic acid is the most abundant

dicarboxylic acid (Kawamura et al., 1996a, b; Yu et al., 2005). Primary sources of oxalic acid exist (e.g., fossil fuel combustion), however they are insufficient to support measured ambient concentrations (Yu et al., 2005). There is growing evidence from atmospheric observations that oxalic acid is a product of cloud processing (Kawamura and Gagosian, 1987; Kawamura and Usukura, 1993; Chebbi and Carlier, 1996; Crahan et al., 2004; Yu et al., 2005; Sorooshian et al., 2006; Heald et al., 2006). For example, Crahan et al. (2004) measured in-cloud and below-cloud oxalate in the coastal marine atmosphere and found that, as for sulfate with a known in-cloud production mechanism, the in-cloud concentration was approximately three times the below-cloud concentration and the size distributions of sulfate-containing and oxalate-containing particles were similar. Sorooshian et al. (2006) compared measured and modeled in-cloud oxalate concentrations from the International Consortium for Atmospheric Research on Transport and Transformation (ICARTT) study and concluded that cloud processing was the major source of atmospheric oxalate. They observed that (1) the detection frequency and particulate oxalate concentration in cloud-free air parcels were significantly lower than for samples collected in-cloud, (2) the highest oxalate concentrations (aerosol and droplet residuals) were observed in clouds influenced by anthropogenic plumes, and (3) sulfate and oxalate were correlated though they are not linked by production chemistry.

Current aqueous-phase models that predict in-cloud oxalic acid formation from GLY assume GLY is oxidized to glyoxylic acid and subsequently to oxalic acid (shaded pathway, Fig. 1). However, organic product analysis in previous GLY aqueous oxidation experiments was limited to glyoxylic acid (Buxton et al., 1997); oxalic acid formation was not confirmed, nor was the potential formation of other low volatility products investigated. The controlled laboratory experiments and product analysis presented below demonstrate the formation of oxalic acid and other low volatility products from aqueous photooxidation of GLY at pH values typical of clouds. Detailed product analysis was used to identify major mechanistic revisions that enabled accurate prediction of oxalic acid formation in the reaction vessel. The expanded reaction mechanism can be used to refine cloud chemistry models. The formation of low volatility species through aqueous photooxidation of GLY provides support to the hypothesis that SOA forms through cloud processing.

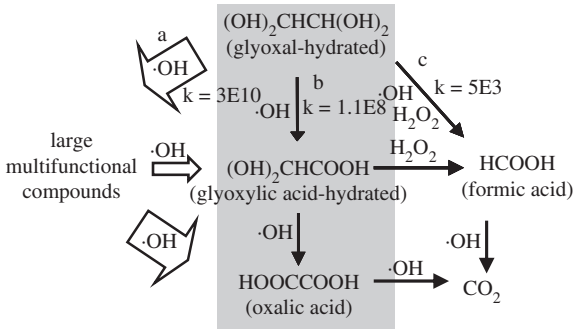

Fig. 1. Aqueous-phase glyoxal oxidation pathways. Glyoxal, glyoxylic acid and glyoxylate are predominantly hydrated in solution (Ervens et al., 2003b). The initial mechanism (pathway "b", shaded) is adapted from Ervens et al. (2004). Pathways "a" and "c" are supported by experimental evidence contained herein.

Table 1
Glyoxal experimental design

Initial glyoxal conc.	2 mM
Initial H_2O_2 conc.	10 mM
Number of experiments	2
pH	4.1–4.8
Temperature	25 ± 1 °C
Experiment	GLY + UV + H_2O_2
UV control	GLY + H_2O_2
H_2O_2 control	GLY + UV
Organic control	UV + H_2O_2

Note: GLY = glyoxal.

2. Methods

2.1. Batch reactions

Batch photochemical aqueous reactions of GLY and hydrogen peroxide were conducted as described previously in detail (Carlton et al., 2006). Experimental conditions are listed in Table 1. UV photolysis of hydrogen peroxide (H_2O_2) provided a source of $^{\bullet}OH$ for GLY oxidation. The UV source was a low-pressure monochromatic (254 nm) mercury lamp (Heraeus Noblelight, Inc. Duluth, GA) in a quartz immersion well in the center of a 1 L borosilicate reaction vessel (ACE Glass Inc., Vineland, NJ). For each experiment (GLY + UV + H_2O_2), three types of control experiments were performed: (1) GLY + H_2O_2 without UV, (2) GLY + UV without H_2O_2, and (3) H_2O_2 + UV without GLY.

Reaction solutions were prepared in 1 L volumetric flasks and then poured into the reaction vessel. Solutions were continuously mixed, maintained at constant temperature and ambient UV penetration was minimized. All experiments began with oxygen-saturated solutions. Samples for H_2O_2 and organic analysis were taken as follows. The first sample was taken directly from the volumetric flask. The second sample was taken immediately after the solution transfer to the reaction vessel, with a third sample taken after 5 min. Samples were then taken at ~10 min intervals for the 1 h experiment (Experiment 1) and ~30 min intervals, with an extra sample during the first hour, for the 5+ h experiment (Experiment 2). H_2O_2 in the experiment and control samples was destroyed through the addition of catalase ($H_2O_2 \rightarrow H_2O$) (0.25 μL 1 mL^{-1} of sample) immediately after sampling (Stefan et al., 1996). Samples were stored frozen until analysis.

Initial GLY concentrations in the experiments were greater than those typically found in cloud and fog droplets (Matsumoto et al., 2005), but concentrations this high have occasionally been observed in the ambient atmosphere (Munger et al., 1995). It is worth noting also that cloud droplet evaporation leaves aerosol particles with very concentrated aqueous solutions (i.e., exceeding concentrations used in these experiments). End products and reaction rate constants for GLY experiments are not expected to be concentration dependent below 1 M (above 1 M, GLY polymerizes) (Whipple, 1970; Kunen et al., 1983; Hastings et al., 2005).

Reaction solutions were prepared with excess oxidant in order to have pseudo-first-order kinetics with regard to GLY. However, initial oxidant levels were limited by the need to keep quenching times (i.e., time to completely destroy H_2O_2 in the samples) short and maintain laboratory safety (e.g., by using H_2O_2 concentrations and H_2O_2-to-catalase ratios that have been previously employed; Stefan et al., 1996). The quenching time was less than 2 min for the first sample and sharply decreased with time as the H_2O_2 concentration in the reaction solutions decreased. Initial modeling using state-of-the-art aqueous-phase mechanisms for GLY (Ervens et al., 2004; Lim et al., 2005) suggested that the initial conditions of Table 1 would yield intermediate and end product concentrations that would be sufficiently above detection limits on the time scale of the experiments.

2.2. Analytical procedures

2.2.1. High-performance liquid chromatography (HPLC)– UV/Vis analysis of organic acids

Organic acid analysis is described in detail in the supporting information of Carlton et al. (2006). Briefly, all standards and samples were analyzed in triplicate for carboxylic acids by HPLC with UV absorbance detection at 205 nm (Beckman Coulter, System Gold, Fullerton, CA). The HPLC employed an Alltech, organic acid ion exclusion column (OA 2000) with the corresponding guard column. The stationary phase was sulfonated polystyrene divinylbenzene and is specifically designed to retain only compounds with organic acid and/or alcohol functional groups (www.alltechweb.com). Compounds containing multiple functional groups are expected to interact with the column multiple times and generate broad peaks, according to column specifications. Compounds without these functionalities, should they be present, are not retained by the column and elute immediately. In the chromatogram unretained products are contained within the void volume, the initial peak associated with sample injection. The mobile phase was H_2SO_4 (pH = 2.3); the flow rate was 0.7 mL min^{-1} and the column temperature was maintained at 45 °C. The mean absorbance (±1 standard deviation of triplicate analyses) was used for quantitation. Multivariate calibration was used to quantify organic acids analyzed by HPLC–UV. Partial least squares (PLS) regression models (Martens and Naes, 1989) were built from concentrations and chromatograms of calibration standards spanning the range of sample concentrations and applied to experimental samples using Statistical Analysis System software (SAS, V8.2, Cary, NC). A set of 25 calibration mixtures with orthogonal concentrations (Brereton, 1997) was used to quantify glyoxylic and oxalic acid. Formic and acetic acids were calibrated with single component standards at five concentration values. GLY and catalase were analyzed alone and added to 12% of the calibration standards. Neither was detected in the chromatograms, and chromatograms of standards with and without GLY and catalase were indistinguishable. (GLY was detected by electrospray ionization–mass spectrometry, ESI–MS; see below.) Ten percent of the mixture standards were re-analyzed and independent single component standards were analyzed to assess analytical accuracy. Recoveries for individual acids were calculated by placing standards in the reaction

vessel and sampling the solution as for experimental samples. Ten percent of experiment samples were collected in duplicate to determine method precision.

2.2.2. Hydrogen peroxide (H_2O_2)

H_2O_2 in the time series samples was quantified by the triiodide method (Klassen et al., 1994) within 1 h of sampling. Solutions were prepared according to Allen et al. (1952) and were not stored longer than 1 month. Calibration was performed with 5 H_2O_2 concentration values and a blank of milli-Q water (18 MΩ). All samples were analyzed in triplicate, one calibration standard was re-analyzed after sample analysis and one independent standard was analyzed during calibration. Method detection limits were determined from analysis of 8 independent blank solutions, 8 times.

2.2.3. Photon flux

The lamp intensity was measured before and after the GLY experiments using iodide–iodate actinometry (Rahn et al., 2003). Briefly, a 1 L actinometer solution of 0.6 M KI, 0.1 M KIO_3 and 0.01 M $Na_2B_4O_7 \cdot 10H_2O$ (borax) at pH 9.25 is prepared immediately prior to the photon flux measurement. The reactor is filled with actinometer solution and exposed to the mercury lamp. Samples are collected as quickly as possible (~every 40 s). The absorbance of the solution is measured immediately with a spectrometer at 476 nm. An absorbance blank of milli-Q water was subtracted from the sample absorbances for photon flux calculations, described below. The intensity of the irradiation source received by solutions in the reaction vessel was calculated using the method described by Murov (1973).

2.2.4. ESI–MS

Selected samples were analyzed by ESI/MS (HP-Agilent 1100) as described previously (Seitzinger et al., 2005; Altieri et al., 2006). Qualitative ESI results are presented here. An autosampler injected sample solutions (20 μL) from individual vials into a liquid chromatography (LC) system, which introduces the sample into the ESI source region. All samples were analyzed with no LC column attached. The mobile phase was 60:40 v/v 100% methanol and 0.05% formic acid in deionized water with a flow rate of 0.220 mL min^{-1}. Samples were analyzed in the negative and positive mode over the mass range 50–1000 amu with a fragmentor voltage of 40 V and a capillary voltage of 3000 V. Nitrogen was the drying gas (350 °C, 24 psig, 10 L min^{-1}). The unit mass resolution spectra were recorded on Agilent software (Chemstation version A.07.01) and exported to Access and Excel (Microsoft, Inc.) for statistical analysis and interpretation.

The ESI–MS uses a soft ionization process that does not fragment compounds at the low voltages used and provides molecular weight information with unit mass resolution. The positive ionization mode protonates compounds with basic functional groups (e.g. methyl, carbonyl) while the negative ionization mode deprotonates compounds with acidic functional groups (e.g. carboxylic acids). Single and mixed standards of GLY, glyoxylic acid and oxalic acid (plus H_2O_2 at a 1:2 ratio and catalase (0.5%)) were analyzed using the same instrument conditions as the experimental samples (see Supporting Information, Figure S-1). Oxalic acid (m/z 89) and glyoxylic acid (m/z 73) were detected as monomers in the negative mode as would be expected for carboxylic acids (Figure S-1). GLY was detected in the positive mode as a dimer (m/z 117; twice molecular weight plus one). Aldehyde dimerization is common during ESI analysis, in particular for GLY (Hastings et al., 2005; Loeffler et al., 2006). In addition to the GLY dimer ion, a second qualifying ion (m/z 131) was detected for GLY. The composition of this ion is unknown, but it appears in concert with the main GLY ion, and linearly increases in ion abundance when GLY concentration increases. The qualifier ion was used for identification purposes only.

2.2.5. Dissolved organic carbon (DOC), pH, dissolved oxygen and temperature

Samples were analyzed for bulk DOC using a Shimadzu 5000A high-temperature combustion analyzer (Sharp et al., 1993). The initial and final pH (Oakton Instruments Vernon Hills, IL) and dissolved oxygen (DO; YSI Inc., Yellowsprings, OH) concentrations were also measured. The pH meter was calibrated at pH = 4, 7, and 10; verification standards (pH = 2, H_2SO_4; pH = 3, $HClO_4$) were analyzed each day of use. DO readings were verified daily using O_2-saturated solutions with known saturation values. Temperature was measured throughout the experiment with an alcohol thermometer that was verified ±2 °C at two temperatures.

2.3. Modeling

Carboxylic acid concentration time profiles were predicted using a commercially available differential equation solver (FACSIMILE; AEA Technology, Oxfordshire, UK). Initial kinetic modeling was based on the aqueous-phase mechanism of Ervens et al. (2004), which is summarized in Fig. 1 (shaded pathway) and reactions 1–16 in Table 2. The corollary anion reactions and the acid/base equilibria are not depicted in Fig. 1 though they occur (Stefan et al., 1996; Ervens et al., 2003a, b) and were included in the model. The concentration of $^{\bullet}OH$ was not explicitly measured; the $^{\bullet}OH$ concentration time series was predicted (Table 2, reactions 1–4; Liao and Gurol, 1995) and the accuracy of these predictions was verified with H_2O_2 measurements as shown below. After examination of the concentration dynamics of products, an expanded reaction mechanism was proposed (all pathways, Fig. 1; all reactions, Table 2). The expanded mechanism, measured concentrations and the differential equation solver were used to fit unknown reaction rate constants and predict the formation of newly identified products.

3. Quality control results

3.1. Organic measurements

The HPLC analysis was used for identification and quantification of compounds, while the ESI–MS analysis was used only for identification of compounds. The PLS and single-acid calibrations described more than 96% of the variance in concentration of each carboxylic acid in the complex mixture standards analyzed by the HPLC. Quality control measures for organic acids are given in Table 3. Recoveries were high, and the lowest recovery (80%) was obtained for the most volatile compound (formic acid) as expected. (Formic acid concentrations were corrected for recoveries.) Method detection limits were determined from analysis of eight "organic control" (i.e., H_2O_2 and UV) samples (Greenberg et al., 1991). Method precision is the pooled coefficient of variation of concentrations measured in duplicate samples. Accuracy was calculated as the percent difference between the actual and measured concentrations of independent standards of individual compounds not used in the calibration models. In the ESI–MS, GLY (m/z 117, 131) was detected in the positive mode, while glyoxylic acid (m/z 73) and oxalic acid (m/z 89) were detected in the negative mode. Note that formic acid has a molecular weight below the ESI–MS instrument detection limit (m/z 50). The ESI–MS and HPLC control experiment results are provided in Supporting Information.

3.2. Photon flux

The calculated mean intensities from photon fluence measurements conducted before and after the GLY experiments agreed within one standard deviation. Hence, these experiments demonstrated that the received lamp intensity was constant during the experiments and the H_2O_2 photolysis reaction rates (reaction 1 in Table 2) were constant across the experiments. The photolysis reaction rate constant (k_1 in Table 2) was determined as described below.

3.3. Hydrogen peroxide (H_2O_2)

The photolytic decomposition of H_2O_2 to $^{\bullet}OH$ in pure water is well understood (Liao and Gurol, 1995; Stefan et al., 1996) and is described in the first 4 reactions of Table 2. H_2O_2 concentrations from H_2O_2 + UV control experiments ($N = 2$) and model predictions agree well (Fig. 2) providing confidence that concentrations of $^{\bullet}OH$ are described well in the experiments. (Note that reaction rate constants k_2–k_4 are known and the photolysis rate (k_1) depends on photon fluence from the lamp and was a fitted parameter.) While experimental and control solutions were prepared with 10 mM H_2O_2, an H_2O_2 concentration of 8 mM was used to initialize the model simulation because H_2O_2 concentrations in the GLY + H_2O_2 control experiments were stable at ~8 mM (see Supporting Information, Figure S-2). This is reasonable because H_2O_2 photolyzes to $^{\bullet}OH$ at wavelengths (λ) present in ambient light and the solution was exposed to ambient light for the ~3-4 min required for solution preparation and transfer into the shielded reaction vessel. H_2O_2 was not detected in the GLY + UV control samples. H_2O_2 photodecomposition experiments (H_2O_2 + UV) have also been performed at an initial H_2O_2 concentration of 20 mM (i.e., as part of the pyruvic acid experiments; Carlton et al., 2006). The model also successfully reproduced these measurements. These experiments provided a photolysis reaction rate constant of $1.0(\pm 0.2) \times 10^{-4}\,s^{-1}$, which was used in model simulations (Table 2, reaction 1) and

Table 2
Glyoxal oxidation mechanism (initial: reactions 1–16; expanded: reactions 1–28)

	Reaction	Rate constant ($M^{-1}\,s^{-1}$)	Reference	Estimated, measured or fitted
1	$H_2O_2+h\nu \rightarrow 2OH$	1.0E−4 (s^{-1})	Liao and Gurol (1995)	m[a]
2	$OH+H_2O_2 \rightarrow HO_2+H_2O$	2.7E+07, 2.7E+10	Liao and Gurol (1995)	m, f[b]
3	$HO_2+H_2O_2 \rightarrow OH+H_2O+O_2$	3.7	Liao and Gurol (1995)	m
4	$HO_2+HO_2 \rightarrow H_2O_2+O_2$	8.3E+05	Liao and Gurol (1995)	m
5	$GLY+OH \rightarrow GLYAC+HO_2$	1.1E+09/1.1E+08	Buxton et al. (1997)	m, f
6	$GLYAC+OH \rightarrow OXLAC+HO_2+H_2O$	3.6E+08	Ervens et al. (2003b)	m
7	$GLYAC^-+OH \rightarrow OXLAC^-+HO_2+H_2O$	2.6E+09	Ervens et al. (2003b)	m
8	$OXLAC+2OH \rightarrow 2CO_2+2H_2O$	1.4E+06	Ervens et al. (2003b)	m
9	$OXLAC^-+OH \rightarrow CO_2+CO_2^-+2H_2O$	1.9E+08/2.2E+08	Ervens et al. (2003b)	m[c]
10	$OXLAC^{2-}+OH \rightarrow CO_2+CO_2^-+OH^-$	1.6E+08	Ervens et al. (2003b)	m
11	$CO_2^-+O_2 \rightarrow O_2^-+CO_2$	2.4E+09	Buxton et al. (1988), Warneck (2003)	m
12	$H_2O = H^++OH^-$	K_{eq} = 1.0E−14, k_a = 1.4E11	Warneck (1999), Lelieveld and Crutzen (1991)	m
13	$HO_2 = Hp1+O_2^-$	K_{eq} = 1.6E−5, k_a = 5.0E10	Warneck (1999, Ervens et al. (2003a)	m, e
14	$GLYAC = H^++GLYAC^-$	K_{eq} = 3.47E−4, k_a = 2.0E10	Warneck (2003), Ervens et al. (2003a)	m, e
15	$OXLAC = H^++OXLAC^-$	K_{eq} = 5.67E−2, k_a = 5.0E10	Warneck (2003), Ervens et al. (2003a)	m, e
16	$OXLAC^- = H^++OXLAC^{2-}$	K_{eq} = 5.42E−5, k_a = 5.0E10	Warneck (2003), Ervens et al. (2003a)	m, e
17	GLY + 2OH → HCO_2H+HCO_2H	5.0E+03	n/a	f
18	$HCO_2H+OH \rightarrow CO_2+HO_2+H_2O$	1.3E+08	Ervens et al. (2003b)	m
19	$HCO_2^- + OH \rightarrow CO_2^- + H_2O$	3.2E+09	Ervens et al. (2003b)	m
20	$HCO_2H = HCO_2^- + H^+$	K_{eq} = 1.77E−4, k_a = 5.0E10	Ervens et al. (2003b)	m, e
21	GLY + OH → Products	3.E+10	n/a	f[d]
22	Products + OH → OXLAC	3.E+10	n/a	f[d]
23	Products + OH → GLYAC	1.E+09	n/a	f[d]
24	$GLY+H_2O_2 \rightarrow HCO_2H+HCO_2H$	1	n/a	f
25	$GLYAC+H_2O_2 \rightarrow HCO_2H+CO_2+H_2O$	0.9	n/a	f[e]
26	$HCO_2H+H_2O_2 \rightarrow CO_2+H_2O$	0.2	n/a	f[e]
27	$OXLAC+H_2O_2 \rightarrow 2CO_2$	0.11	n/a	f[e]
28	$OXLAC^- \rightarrow 2CO_2$	1.5E−04	n/a	f[e]

Notes: Reactions 1–16 (italicized), used in initial mechanism, Reactions 17–28 added for expanded mechanism.
GLY = glyoxal, GLYAC = glyoxylic acid, OXLAC = oxalic acid, OH = $^{\bullet}$OH; m = measured, e = estimated, f = fitted; dissociation rate constants (k_d) are calculated from the equilibrium constant (K_{eq}; i.e., $k_d = K_{eq} \times k_a$).

[a] k_1 is a fitted parameter with observations fit to the Liao and Gurol (1995) parameterization.

[b] Modeling was performed with $k_2 = 2.7E+10$, which likely represents the net rate of several reactions: $OH + H_2O_2 \rightarrow HO_2 + H_2O$; $OH + HO_2 \rightarrow H_2O + O_2$ (1.1E10, Elliot and Buxton (1992)); $OH + RO_2 \rightarrow$ products (~E10). Note that H_2O_2 was insensitive to the choice of k_2 (measured vs. fitted).

[c] This reaction rate constant is within the uncertainty of the measured value present by Ervens et al. (2003b) ($k = 1.9(\pm 0.6)E+08$).

[d] These simplified reactions are surrogates for unknown formation processes.

[e] These fitted reaction rate constants for H_2O_2 reaction with carboxylic acids are reasonable and close in value to the measured reaction rate constant for pyruvic acid + H_2O_2 (0.11 M s^{-1}; Stefan and Bolton (1999)).

Table 3
Carboxylic acid quality control measures

	Formic acid	Glyoxylic acid	Oxalic acid
Recovery	80% ($N = 2$)	90% ($N = 2$)	100% ($N = 2$)
Method detection limit	0.07 mM ($N = 8$)	0.12 mM ($N = 8$)	0.06 mM ($N = 8$)
Method precision		Pooled C.V. = 17%, $N = 5$	
Accuracy	15% ($N = 2$)	10% ($N = 3$)	5% ($N = 3$)

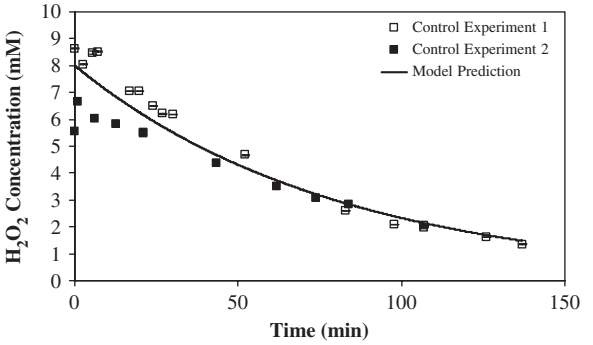

Fig. 2. Hydrogen peroxide measurements and model predictions. The photolysis rate constant for $H_2O_2 \rightarrow 2^{\bullet}OH$, ($1.0E{-}04\,s^{-1}$), was a fitted parameter (see Table 2, reaction 1). Note that the H_2O_2 model concentration at $t = 0$ was considered to be equal to the H_2O_2 concentration observed throughout the GLY + H_2O_2 control experiment (Figure S-2). This accounts for H_2O_2 photolysis due to ambient UV during solution preparation.

is similar to values obtained by others conducting similar experiments (Herrmann et al., 1995).

4. Experimental results

4.1. Concentration dynamics

GLY (m/z 117, 131) was present in the 0 min sample and was completely absent by 9 min as demonstrated in the ESI mass spectra (Fig. 3). This decrease in GLY coincided with the very rapid formation of formic acid (Fig. 4; HPLC retention time (RT) 3.3 min). The formic acid concentration reached a maximum within the first 2 min of the experiment (Fig. 4); it was not a predicted product. Glyoxylic acid, an expected product (Fig. 1), has a maximum HPLC absorbance at 9 min, however observations never exceeded detection limits (Figs. 4 and 5). Total DOC decreased by approximately a factor of 10 within the first hour.

In addition to the compounds predicted in the initial reaction scheme (shaded pathway, Fig. 1), the formation of larger molecular weight compounds

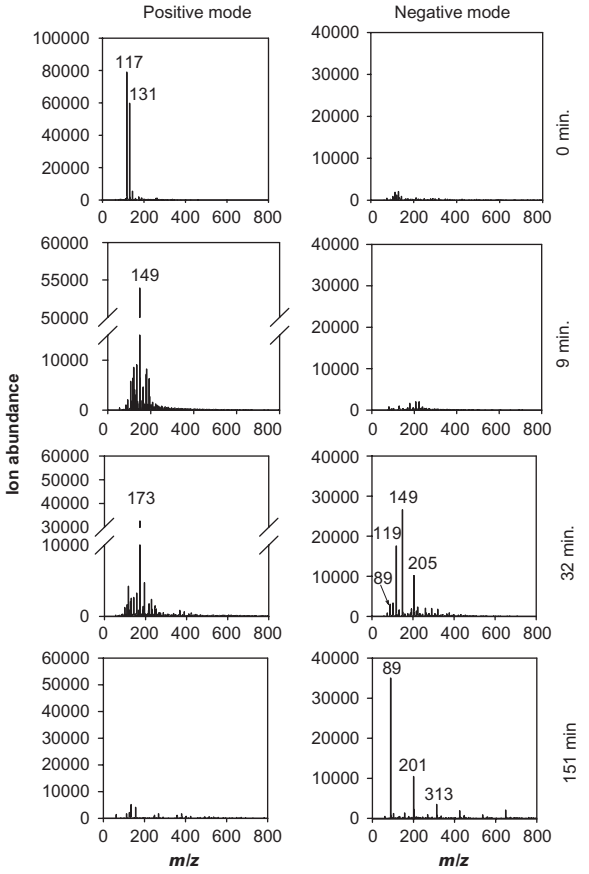

Fig. 3. ESI mass spectra of selected samples from experiment 2 with increasing reaction time. Note change in y-axis scale for the first positive mode spectrum. Glyoxal (m/z 117, 131) is clearly present in the 0 min sample. Oxalic acid (m/z 89) is clearly present in the 151 min spectrum. Molecular level identification of other products will require higher-resolution ESI–MS or other complementary analytical techniques.

was evident in both the HPLC chromatograms and the ESI mass spectra. By ~9 min the positive mode ESI–MS spectra showed numerous peaks clustered between m/z 80–200 (Fig. 3). At ~30 min, there still were higher molecular weight peaks in the positive mode spectra and, in addition, there were higher molecular weight peaks in the negative mode

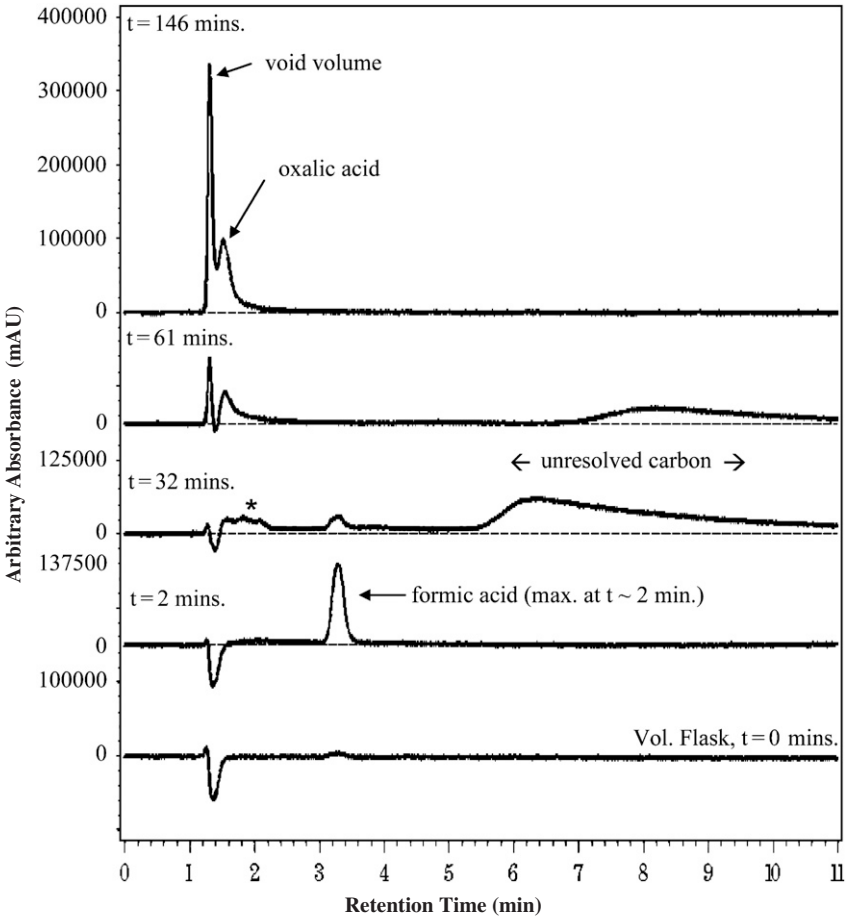

Fig. 4. HPLC chromatograms of selected samples from experiment 2. Oxalic acid plateaus at ~50–150 min and is the only product observed in the chromatograms after the 146 min sample. Formic acid appears quickly and is no longer present after the 32 min sample. The unresolved carbon maximum occurs at ~30 min. Note: mAU = milli-absorbance units; *indicates the small glyoxylic acid presence in the 32 min sample. Note that the *y*-axis units are arbitrary absorbance units. Note that unretained species are included in the void volume peak.

spectra. After ~30 min, the complexity in the spectra of both positive and negative modes dissipated. (Note: the simple mass spectra of controls and mixture standards containing all expected products, shown and discussed in Supporting Information, provides strong evidence that the ESI–MS "complexity" is not an instrumental artifact.) A feature with the same temporal evolution was found in the HPLC chromatograms (Fig. 4). The HPLC chromatograms exhibited a broad peak with a long retention time whose area reached a maximum at ~30 min (Fig. 4). The broad peak suggests the formation of larger, multifunctional products, and the long retention time suggests relatively high pK_a values (typical of alcohols). After 30 min, the retention time of this peak increased (shifted from 6.4 to 8 min) and the peak area decreased. Column characteristics indicate that the shift to a longer retention time is most likely associated with an increase in compound pK_a, or molecular size. The decrease in area strongly suggests a decrease in concentration, however this is not explicitly known since the analytical sensitivity could change with the changing product mix. A dramatic increase in the oxalic acid concentration occurred after 30 min (Figs. 3–5), as the ESI–MS "complexity" dissipated and the broad peak of unresolved carbon in HPLC chromatograms decreased. Glyoxylic acid concentrations are insufficient to account for this increase in oxalic acid. Concentration dynamics suggest that the degradation of larger multifunctional compounds is somehow responsible. The oxalic acid concentration reached a plateau at 50–150 min (HPLC,

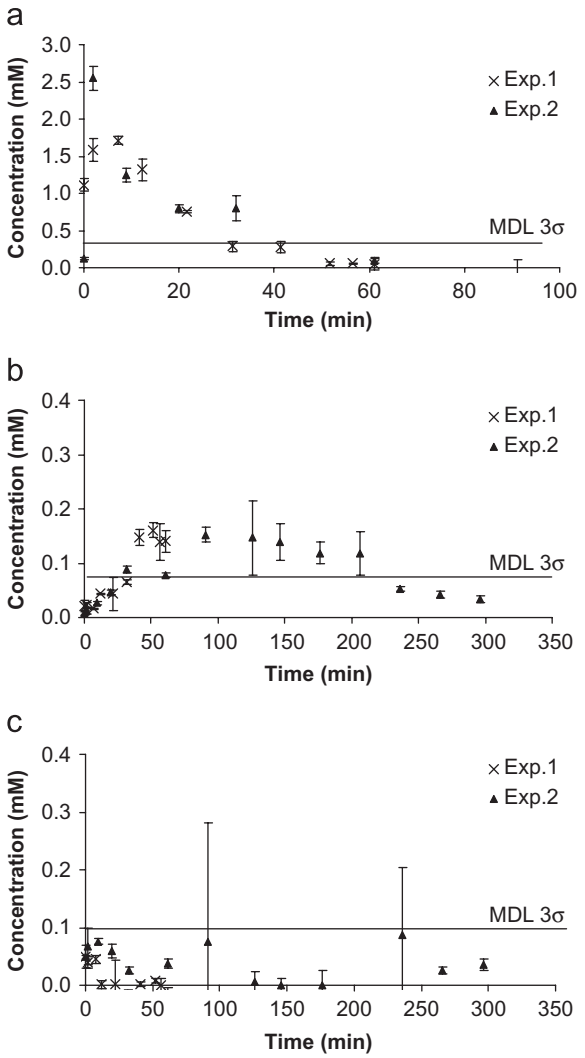

Fig. 5. Formic acid (a), oxalic acid (b), and glyoxylic acid (c) concentration in glyoxal experiments. The experiments had good repeatability; carboxylic acid concentrations across experiments were within measurement uncertainties. MDL is method detection limit.

RT = 1.5 min; ESI–MS, m/z 89 negative mode) (Figs. 3–5). After 150 min, oxalic acid was the only peak present in the chromatograms and dominated the ESI mass spectra as its concentration gradually decreased.

4.2. Modeling organic acid formation

These experiments demonstrate that while oxalic acid does form from aqueous-phase photooxidation of GLY, as expected, the mechanism is more complex than previously thought. Larger multifunctional compounds and rapid formic acid formation and degradation were not predicted by the original mechanism, and the current experiments suggest that glyoxylic acid oxidation is not the predominant oxalic acid formation pathway. Published atmospheric aqueous-phase models predict oxalic acid production from GLY via glyoxylic acid (pathway b; Fig. 1). While glyoxylic acid oxidation could explain the initial formation of oxalic acid, glyoxylic acid concentrations are insufficient to account for the substantial oxalic acid growth after 30 min. Oxalic acid forms rapidly as the broad HPLC peak suggestive of larger multifunctional compounds decreases and as the ESI mass spectral complexity decreases, suggesting that oxalic acid forms primarily through the degradation of a class of larger multifunctional compounds (pathway a; Fig. 1).

The model using the initial mechanism (Table 2, reactions 1–16) failed to reproduce the concentrations of measured species or their temporal dynamics in the experiments (Fig. 6). Over-prediction of glyoxylic acid concentrations has been reported for previous GLY photooxidation experiments as well (Buxton et al., 1997).

Based on the experimental results, the original mechanism (shaded pathway, Fig. 1) was expanded to include the formation and degradation of formic acid and larger molecular weight compounds (all pathways, Fig. 1). Table 2 presents the reactions and fitted rate constants used in the expanded mechanism model. Reactions were added for formic acid formation, dissociation and oxidation (reactions 17–20, 24–26). The rapid formation of formic acid very early in the time series suggests it is a direct GLY oxidation product; its

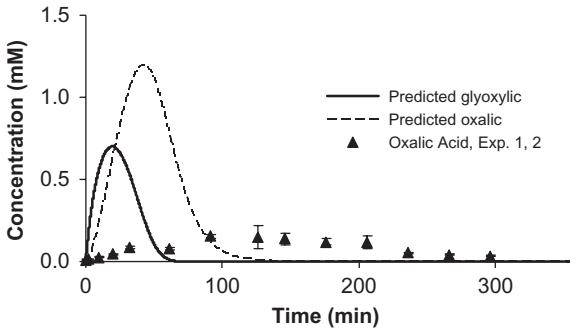

Fig. 6. Measured and predicted concentrations of oxalic acid using initial mechanism (shaded pathway, Fig. 1; Table 2, reactions 1–16). Note that observed glyoxylic acid concentrations are all below detection limits (Fig. 5).

concentration dynamics could not be reproduced until the reactions $GLY + 2^{\bullet}OH \rightarrow 2HCOOH$ and $GLY + H_2O_2 \rightarrow 2HCOOH$ (reactions 17 and 24) were added to the expanded mechanism. The first reaction is reasonable because α-dicarbonyl compounds are highly reactive, and the proximity of the two carbonyl double bonds enhances their reactivity toward nucleophilic (e.g., $^{\bullet}OH$) attack (Vollhardt and Schore, 1994). The second reaction route is supported by substantial experimental evidence (Gavagan et al., 1995; Rao and Rao, 2005; Seip et al., 1993), although, to the best of our knowledge, a rate constant for this reaction is not provided in the literature. The expanded mechanism therefore includes direct formic acid production from GLY through reactions with $^{\bullet}OH$ and H_2O_2 (pathway c, Fig. 1). Reactions were added (reactions 21–23) to parameterize the formation and degradation of a class of larger multifunctional intermediates (i.e., the unresolved carbon) that appear to be responsible for most of the oxalic acid formation. These simplified reactions do not explicitly characterize the products, as they are unknown and appear to change with time. The rate constants (k_{21}–k_{23}) were adjusted so that model predictions fit the observed concentrations of quantified species (e.g., formic and oxalic acids). Fitting was not directly possible for the "higher molecular weight compounds" because they are unidentified and therefore calibration relationships cannot be calculated. However, the model fit for quantifiable species was excellent and these calculated rate constants are consistent with other investigators who note that aqueous-phase reaction rate constants involving the hydroxyl radical occur at or near diffusion limits (i.e., $\sim 10^{10}\,M^{-1}\,s^{-1}$) (Haag and Yao, 1992; Zhu and Nicovich, 2003). For both the original mechanism and the expanded mechanism, initial concentrations of H_2O_2 and $^{\bullet}OH$ were optimized at 9 and 0.15 mM, respectively, reflecting the fact that some H_2O_2 photolyzes to $^{\bullet}OH$ during solution preparation (see Supporting Information). Additionally, organic reactions with H_2O_2 were added to the model (reactions 25–28). Including these reactions is reasonable because pyruvic (Stefan and Bolton, 1999; Carlton et al., 2006) and glyoxylic acids (Seip et al., 1993; Gavagan et al., 1995; Rao and Rao, 2005) have been shown to react with H_2O_2. Their inclusion improved model performance for the experiments and controls. Note that k_2 exceeds the published rate constant for reaction 2 (Table 2) and likely represents the net rate of several reactions involving peroxy compounds. Oxalic acid and $^{\bullet}OH$ (but not H_2O_2) are sensitive to the choice of k_2.

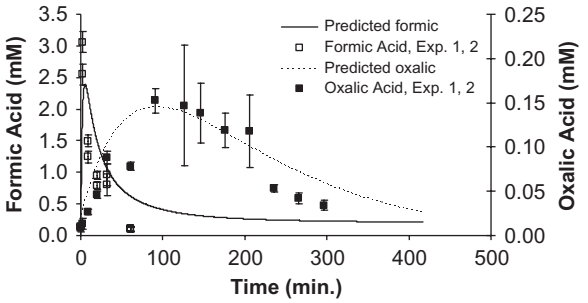

Fig. 7. Measured and predicted concentrations of formic (left axis) and oxalic (right axis) acids using expanded mechanism (all pathways, Fig. 1; Table 2, reactions 1–28). Glyoxylic acid concentrations are too small (<0.02 mM) to see at this scale. Glyoxal is below detection limits by the 9 min sample.

Using the expanded mechanism (Fig. 1) and reactions 1–28 (Table 2) with certain rate constants as fitting parameters (k_2, k_{17}, k_{21}–k_{28}), predicted and measured concentration profiles are in reasonable agreement, and the predictions reproduce the measured concentration dynamics (Fig. 7). The expanded mechanism describes 81% of the variance in oxalic acid observations. Formic acid predictions account for 60% of the variance in observations. This modest agreement for formic acid might be explained by the lower recovery for formic acid or the fact that formic acid appears very rapidly and degrades early in the experiment, when uncertainty in the independent variable (i.e., time) is still a relatively large fraction of the measurement. The predicted glyoxylic acid concentrations using the expanded mechanism are below detection limits, as observed. The expanded model suggests that less than 1% of oxalic acid in the reaction vessel is formed through the glyoxylic acid pathway (pathway b, Fig. 1).

4.3. Model limitations

Reactions 21–23 are surrogates for poorly understood processes that enhance reactant disappearance. For example, GLY could also react with unidentified products (e.g., radicals or larger multifunctional compounds observed in the HPLC and ESI mass spectra). The larger multifunctional products change during the experiment, as indicated by the shifts in the HPLC retention time and as demonstrated by the distribution of mass species in the ESI–MS. Further experimental work to identify

products and their formation mechanisms is required for further model improvement and for accurate prediction of the properties and concentration dynamics of the larger molecular weight products. Prediction of SOA formation through aqueous-phase photochemistry is hampered by the lack of understanding of the thermodynamic properties, atmospheric stability and concentrations of these unknown products.

5. Yields

In these batch reactor experiments, a fixed quantity of GLY was reacted with $^{\bullet}OH$ generated by H_2O_2 photolysis leading to the formation, evolution and eventual destruction of low volatility products. Because the chemical composition in the reaction vessel continues to evolve after all GLY has reacted (9 min), the mass of product per mass of GLY reacted (frequently called the yield) is not a constant, but a function of the reaction time. After 10 min of aqueous-phase processing the reaction vessel contained 0.01 g oxalic acid per g GLY reacted (1%). (Note: 10 min is a typical cloud droplet lifetime and an air parcel might be processed through tens of cloud cycles during regional transport; Ervens et al., 2004.) At the oxalic acid concentration maximum (~90 min), the reaction vessel contained 0.02 g oxalic acid per g GLY reacted (2%). After ~150 min the mass of oxalic acid in the reaction vessel decreased, until all oxalic acid was oxidized to CO_2 (>300 min). Atmospheric yields of oxalic acid (and SOA) from cloud processing of GLY will depend not only on the aqueous-phase chemistry investigated in this research, but also on the rate at which oxidants and GLY are (continuously) supplied by gas-phase chemistry, on photolysis rates, and on cloud dynamics (e.g., cloud contact time).

We expect that the larger multifunctional products formed from aqueous GLY photooxidation will also contribute to SOA. Experimental observations suggest that the maximum higher molecular weight compound concentration occurs at ~30 min, when the median molecular weight in the ESI–MS was ~175 g mol^{-1} (Fig. 3). Using this as the estimated molecular weight, a maximum of 0.3 g higher molecular weight compounds g^{-1} reacted GLY (30%) was estimated for the reaction vessel (~30 min). Note there is substantial uncertainty in this estimate as compounds are unknown and there is uncertainty in the calculated reaction rate constants. Plus, while we expect higher molecular weight material to remain largely in the particle phase upon droplet evaporation (Loeffler et al., 2006), its gas-particle partitioning is not well characterized. However, this value indicates that model investigations of cloud-produced SOA that neglect higher molecular weight compounds (e.g., rely on carboxylic acid production solely) could substantially under-predict SOA formation.

6. Discussion

This work supports the hypothesis that aqueous-phase photooxidation of GLY leads to SOA formation. Oxalic acid formation is confirmed, and an expanded formation mechanism is proposed. The coupled atmospheric concentration dynamics of GLY and oxalic acid (Chebbi and Carlier, 1996), results from recent field campaigns (Crahan et al., 2004; Sorooshian et al., 2006) and this work support the hypothesis that aqueous-phase chemistry is the predominant formation mechanism for oxalic acid. Good agreement is found between measured and modeled oxalic acid concentrations using the expanded mechanism developed herein. This work suggests that larger multifunctional compounds are also products of aqueous-phase GLY photooxidation. Both oxalic acid and larger multi-functional compounds will contribute SOA upon droplet evaporation.

The larger multifunctional products are likely to be covalently bonded oligomers or compounds with relatively high pK_a values and carboxylic acid or alcohol functional groups. The evidence supporting this is as follows: the HPLC column retains only carboxylic acids and alcohols, high pK_a compounds have longer elution times in this column, and multifunctional compounds have broad chromatographic peaks. Also, the complexity in the ESI mass spectra occurs in both the positive (e.g., alcohols) and negative (e.g., carboxylic acids) modes. The formation of larger multi-functional compounds has been reported previously in similar photooxidation experiments of carboxylic acids (e.g., pyruvic acid; Altieri et al., 2006). These compound classes (i.e., alcohols, covalently bonded oligomers and larger carboxylic acids) are consistent with proposed cloud water HULIS (humic-like substances) components (Cappiello et al., 2003). Oligomers and HULIS have been found in atmospheric aerosols (Gao et al., 2006; Kalberer et al., 2004, 2006) and in clouds (Fuzzi et al., 2002; Cappiello et al., 2003).

It has been suggested that these larger compounds form in a concentrated liquid phase (i.e., acidic particles; Tolocka et al., 2004; Kroll et al., 2006), but we provide evidence that larger multi-functional compounds can also form in dilute solutions (i.e., cloud droplets) as suggested by Blando and Turpin (2000) and Gelencser and Varga (2005). Still, further work is needed to better characterize these unidentified products, their formation chemistry and relevant atmospheric properties.

The work presented here demonstrates one of the many complex pathways leading to the formation of SOA through cloud processing. SOA yields from GLY could be substantially higher than oxalic acid yields because oxalic acid is only one of many potential low volatility products. For example, in addition to oxalic acid and larger multifunctional compounds, organosulfur compounds (e.g., GLY–sulfur adducts; Munger et al., 1984, 1995; Liggio et al., 2005) could form and contribute to SOA. Also, while GLY is a gas-phase oxidation product of many VOCs, it is only one of many potential aqueous-phase SOA precursors. Thus, the inclusion of in-cloud SOA formation pathways in chemical transport models is likely to reduce the gap between measured and modeled organic PM in the free troposphere (Heald et al., 2006).

Acknowledgments

The authors gratefully acknowledge useful conversations with Dr. Jeehiun Lee, Dr. John Reinfelder, Yi Tan, and Dr. Mark Perri. This research was supported in part by the US EPA Science to Achieve Results (STAR) program (R831073), the National Science Foundation (NSF-ATM-0630298), an Air & Waste Management Association Air Pollution Research Grant (APERG) and the New Jersey Agricultural Experiment Station and the NOAA Climate Goal. Although the research described in this paper has been funded and reviewed by the US EPA, it does not necessarily reflect the views of the EPA; no official endorsement should be inferred. Any opinions, findings, and conclusions or recommendations expressed in this material are those of the authors and do not necessarily reflect the views of the National Science Foundation.

Disclaimers: The research presented here was performed, in part, under the Memorandum of Understanding between the US Environmental Protection Agency (EPA) and the US Department of Commerce's National Oceanic and Atmospheric Administration (NOAA) and under agreement number DW13921548. This work constitutes a contribution to the NOAA Air Quality Program. Although it has been reviewed by EPA and NOAA and approved for publication, it does not necessarily reflect their policies or views.

Appendix A. Supplementary material

The online version of this article contains additional supplementary data. Please visit doi:10.1016/j.atmosenv.2007.05.035.

References

Allen, A.O., Hochanadel, C.J., Ghormley, J.A., Davis, T.W., 1952. Decomposition of water and aqueous solutions under mixed fast neutron and gamma radiation. Journal of Physical Chemistry 56, 576–586.

Altieri, K.E., Carlton, A.G., Lim, H.J., Turpin, B.J., Seitzinger, S., 2006. Evidence for oligomer formations in clouds: reactions of isoprene oxidation products. Environmental Science and Technology 40, 4956–4960.

Atkinson, R., 2000. Atmospheric chemistry of VOCs and NO_x. Atmospheric Environment 34, 2063–2101.

Atkinson, R., Baulch, D.L., Cox, R.A., Crowley, J.N., Hampson, R.F., Hynes, R.G., Jenkin, M.E., Rossi, M.J., Troe, J., 2006. Evaluated kinetic and photochemical data for atmospheric chemistry: volume II-gas phase reactions of organic species. Atmospheric Chemistry and Physics 6, 3625–4055.

Betterton, E.A., Hoffmann, M.R., 1988. Henry's Law constants of some environmentally important aldehydes. Environmental Science and Technology 22, 1415–1418.

Blando, J.D., Turpin, B.J., 2000. Secondary organic aerosol formation in cloud and fog droplets: a literature evaluation of plausibility. Atmospheric Environment 34, 1623–1632.

Brereton, R.G., 1997. Multilevel multifactor designs for multivariate calibration. Analyst 122, 1521–1529.

Buxton, G.V., Greenstonck, C.L., Hellman, W.P., Ross, A.B., 1988. Journal of Physical Chemistry Reference Data 17, 513.

Buxton, G.V., Malone, T.N., Salmon, G.A., 1997. Oxidation of glyoxal initiated by $^{\bullet}OH$ in oxygenated aqueous solution. Journal of the Chemical Society, Faraday Transactions 93, 2889.

Cappiello, A., De Simoni, E., Fiorucci, C., Mangani, F., Palma, P., Trufelli, H., Decesari, S., Facchini, M.C., Fuzzi, S., 2003. Molecular characterization of the water-soluble organic compounds in fogwater by ESIMS/MS. Environmental Science and Technology 37, 1229–1240.

Carlton, A.G., Lim, H.-J., Altieri, K., Seitinger, S., Turpin, B.J., 2006. Link Between Isoprene and SOA: fate of pyruvic acid in dilute aqueous solution. Geophysical Research Letters 33.

Chebbi, A., Carlier, P., 1996. Carboxylic acids in the troposphere, occurrence, sources and sinks: a review. Atmospheric Environment 30, 4233–4249.

Crahan, K.K., Hegg, D., Covert, D.S., Jonsson, H., 2004. An exploration of aqueous oxalic acid production in the coastal marine atmosphere. Atmospheric Environment 23, 3757–3764.

EPA, US, 2004. Air Quality Criteria for Particulate Matter. US Environmental Protection Agency, Research Triangle Park.

Elliot, A.J., Buxton, G.V., 1992. Temperature dependences of the reactions $OH + O_2^-$ and HO_2 in water upto 200 °C. Journal of the Chemical Society, Faraday Transactions 88, 2465–2470.

Ervens, B., George, C., Williams, J.E., Buxton, G.V., Salmon, G.A., Bydder, M., Wilkinson, F., Dentener, F., Mirabel, P., Wolke, R., Herrmann, H., 2003a. CAPRAM 2.4 (MODAC mechanism): an extended and condensed tropospheric aqueous phase mechanism and its application. Journal of Geophysical Research-Atmospheres 108.

Ervens, B., Gligorovski, S., Herrmann, H., 2003b. Temperature-dependent rate constants for hydroxyl radical reactions with organic compounds in aqueous solutions. Physical Chemistry Chemical Physics 5, 1811–1824.

Ervens, B., Feingold, G., Frost, G.J., Kreidenweis, S.M., 2004. A modeling study of aqueous production of dicarboxylic acids: 1. Chemical pathways and speciated organic mass production. Journal of Geophysical Research 109.

Fuzzi, S., Facchini, M.C., Decesari, S., Matta, E., Mircea, M., 2002. Soluble organic compounds in fog and cloud droplets: what have we learned over the past few years? Atmospheric Research 64, 89–98.

Gao, S., Surratt, J.D., Knipping, E.M., Edgerton, E.S., Shahgholi, M., Seinfeld, J.H., 2006. Characterization of polar organic components in fine aerosols in the southeastern United States: identity, origin, and evolution. Journal of Geophysical Research-Atmospheres 111.

Gavagan, J.E., Fager, S.K., Seip, J.E., Payne, M.S., Anton, D.L., DiComsimo, R., 1995. Glyoxylic acid production using microbial transformant catalysts. Journal of Organic Chemistry 60, 3957–3963.

Gelencser, A., Varga, Z., 2005. Evaluation of the atmospheric significance of multiphase reactions in atmospheric secondary organic aerosol formation. Atmospheric Chemistry and Physics 5, 2823–2831.

Greenberg, A.E., Eaton, A.D., Clesceri, L.S., 1991. American Public Health Association, American Water Works Association, and Water Pollution Control Federation, Standard Methods for the Examination of Water and Wastewater: 1991 Supplement to the 17th Edition. American Public Health Association, Washington, DC, 1449 pp.

Guzman, M.I., Colussi, A.I., Hoffmann, M.R., 2006. Photoinduced oligomerization of aqueous pyruvic acid. Journal of Physical Chemistry A 110, 3619–3626.

Haag, W.R., Yao, C.C.D., 1992. Rate constants for reaction of hydroxyl radicals with several drinking water contaminants. Environmental Science & Technology 26, 1005–1013.

Hastings, W.P., Koehler, C.A., Bailey, E.L., DeHaan, D.O., 2005. Secondary organic aerosol formation by glyoxal hydration and oligomer formation: humidity effects and equilibrium shifts during analysis. Environmental Science and Technology 39, 8728–8735.

Heald, C.L., Jacob, D.J., Park, R.J., Russell, L.M., Huebert, B.J., Seinfeld, J.H., Liao, H., Weber, R.J., 2005. A large organic aerosol source in the free troposphere missing from current models. Geophysical Research Letters 32.

Heald, C.L., Jacob, D.J., Turquety, S., Hudman, R.C., Weber, R.J., Sullivan, A.P., Peltier, R.E., Atlas, E.L., de Gouw, J.A., Warneke, C., Holloway, J.S., Neuman, J.A., Flocke, F.M., Seinfeld, J.H., 2006. Concentrations and sources of organic carbon aerosols in the free troposphere over North America. Journal of Geophysical Research-Atmospheres 111.

Herrmann, H., Reese, A., Zellner, R., 1995. Time-resolved UV/Vis diode-array absorption-spectroscopy of SO_x-(X = 3, 4, 5) radical-anions in aqueous-solution. Journal of Molecular Structure 348, 183–186.

IPCC, 2001. Climate Change 2001: The Scientific Basis. Cambridge University Press, Cambridge, UK.

Kalberer, M., Paulsen, D., Sax, M., Steinbacher, M., Dommen, J., Prevot, A.S.H., Fisseha, R., Weingartner, E., Frankevich, V., Zenobi, R., Baltensperger, U., 2004. Identification of polymers as major components of atmospheric organic aerosols. Science 303, 1659–1662.

Kalberer, M., Sax, M., Samburova, V., 2006. Molecular size evolution of oligomers in organic aerosols collected in urban atmospheres and generated in a smog chamber. Environmental Science & Technology 40, 5917–5922.

Kanakidou, M., Seinfeld, J.H., Pandis, S.N., Barnes, I., Dentener, F.J., Facchini, M.C., Dingenen, R.V., Ervens, B., Nenes, A., Nielsen, C.J., Swietlicki, E., Putaud, J.P., Balkanski, Y., Fuzzi, S., Horth, H., Moortgat, G.K., Winterhalter, R., Myhre, C.E.L., Tsigaridis, K., Vignati, E., Stephaou, E.G., Wilson, J., 2005. Organic aerosol and global climate modelling: a review. Atmospheric Chemistry and Physics 5, 1053–1123.

Kawamura, K., Gagosian, R.B., 1987. Implication of ω-oxocarboxylic acids in the remote marine atmosphere for photo-oxidation of unsaturated fatty acids. Nature 325, 330–332.

Kawamura, K., Usukura, K., 1993. Distributions of low molecular weight dicarboxylic acids in North Pacific aerosol samples. Journal of Oceanography 49, 271–283.

Kawamura, K., Kasukabe, H., Barrie, L., 1996a. Source and reaction pathways of dicarboxylic acids, ketoacids, and dicarbonyls in Arctic aerosols: one year of observations. Atmospheric Environment 30, 1709–1722.

Kawamura, K., Semere, R., Imai, Y., Fujii, Y., Hayashi, M., 1996b. Water soluble dicarboxylic acids and related compounds in Antarctic aerosols. Journal of Geophysical Research-Atmospheres 101, 18721–18728.

Klassen, N.V., Marchinton, D., McGowan, H.C.E., 1994. H_2O_2 determination by the I_3^- method and by $KMNO_4$ titration. Analytical Chemistry 66, 2921–2925.

Kleindienst, T.E., Smith, D.F., Li, W., Edney, E.O., Driscoll, D.J., Speer, R.E., Weathers, W.S., 1999. Secondary organic aerosol formation from the oxidation of aromatic hydrocarbons in the presence of dry submicron ammonium sulfate aerosol. Atmospheric Environment 33, 3669–3681.

Kroll, J.H., Ng, N.L., Murphy, S.M., Flagan, R.C., Seinfeld, J.H., 2006. Secondary organic aerosol formation from isoprene photooxidation. Environmental Science and Technology 40, 1869–1877.

Kunen, S.M., Lazrus, A.L., Kok, G.L., Heikes, B.G., 1983. Aqueous oxidation of SO_2 by hydrogen peroxide. Journal of Geophysical Research 88, 3671–3674.

Lelieveld, J., Crutzen, P.J., 1991. The role of clouds in tropospheric photochemistry. Journal of Atmospheric Chemistry 12, 229.

Liao, C.-H., Gurol, M.D., 1995. Chemical oxidation by photolytic decomposition of hydrogen peroxide. Environmental Science and Technology 29.

Liggio, J., Li, S.M., McLaren, R., 2005. Heterogeneous reactions of glyoxal on particulate matter: identification of acetals and sulfate esters. Environmental Science and Technology 39, 1532–1541.

Lim, H.-J., Carlton, A.G., Turpin, B.J., 2005. Isoprene forms secondary organic aerosol through cloud processing: model simulations. Environmental Science and Technology 39, 4441–4446.

Loeffler, K.W., Koehler, C.A., Paul, N.M., De Haan, D.O., 2006. Oligomer formation in evaporating aqueous glyoxal and methyl glyoxal solutions. Environmental Science and Technology 40, 6318–6323.

Magneron, I., Mellouki, A., LeBras, G., Moortgat, G.K., Horowitz, A., Wirtz, K., 2005. Photolysis and OH-initiated oxidation of glycolaldehyde under atmospheric conditions. Journal of Physical Chemistry A 109, 4552–4561.

Martens, H., Naes, T., 1989. Multivariate Calibration. Wiley, New York.

Matsumoto, K., Kawai, S., Igawa, M., 2005. Dominant factors controlling concentrations of aldehydes in rain, fog, dew water, and in the gas phase. Atmospheric Environment 39, 7321–7329.

Miller, W.L., Moran, M.A., 1997. Interaction of photochemical and microbial processes in the degradation of refractory dissolved organic matter from a coastal marine environment. Limnology and Oceanography 42, 1317–1324.

Munger, J.W., Jacob, D.J., Hoffmann, M.R., 1984. The occurrence of bisulfite-aldehyde addition products in fog- and cloud-water. Journal of Atmospheric Chemistry 1, 335–350.

Munger, J.W., Collett, J., Daube Jr., B.C., Hoffmann, M.R., 1990. Fogwater chemistry at Riverside California. Atmospheric Environment 24, 185–205.

Munger, J.W., Jacob, D.J., Daube, B.C., Horowitz, L.W., 1995. Formaldehyde, glyoxal and methylglyoxal in air and cloud-water at a rural mountain site in central Virginia. Journal of Geophysical Research 100, 9325–9333.

Murov, S.L., 1973. Handbook of Photochemistry. Marcel Decker, Inc., New York.

Rahn, R.O., Stefan, M.I., Bolton, J.R., Goren, E., Shaw, P.S., Lykke, K.R., 2003. Quantum yield of the iodide–iodate chemical actinometer: dependence on wavelength and concentration. Photochemistry and Photobiology 78, 146–152.

Rao, T.S., Rao, M.S.P., 2005. Titrimetric and spectrophotometric methods for the determination of glyoxal and analysis of ternary mixtures of its oxidation products. Journal of Analytical Chemistry 60, 714–718.

Schweitzer, F., Magi, L., Mirabel, P., George, C., 1998. Uptake rate measurements of methanesulfonic acid and glyoxal by aqueous droplets. Journal of Physical Chemistry A 102, 593–600.

Seinfeld, J.H., Pandis, S.N., 1998. Atmospheric Chemistry and Physics. Wiley, New York.

Seip, J.E., Fager, S.K., Gavagan, J.E., Gosser, L.W., Anton, D.L., DiCosimo, R., 1993. Biocatalytic production of glyoxylic acid. Journal of Organic Chemistry 58, 2253–2259.

Seitzinger, S.P., Hartnett, H., Lauck, R., Mazurek, M., Minegishi, T., Spyres, G., Styles, R., 2005. Molecular-level chemical characterization and bioavailability of dissolved organic matter in stream water using electrospray-ioniation mass spectrometry. Limnology and Oceanography 50, 1–12.

Sempere, R., Kawamura, K., 1994. Comparative distributions of dicarboxylic acids and related polar compounds in snow, rain and aerosols from urban atmosphere. Atmospheric Environment 28, 449–459.

Sharp, J.H., Benner, R., Bennett, L., Carlson, C.A., Dow, R., Fitzwater, S.E., 1993. Reevaluation of high temperature combustion and chemical oxidation measurements of dissolved organic-carbon in seawater. Limnology and Oceanography 38, 1774.

Sorooshian, A., Varutbangkul, V., Brechtel, F.J., Ervens, B., Feingold, G., Bahreini, R., Murphy, S.M., Holloway, J.S., Atlas, E.L., Buzorius, G., Jonsson, H., Flagan, R.C., Seinfeld, J.H., 2006. Oxalic acid in clear and cloudy atmospheres: analysis of data from ICARTT 2004. Journal of Geophysical Research-Atmospheres 111, D23S45.

Spaulding, R.S., Schade, G.W., Goldstein, A.H., Charles, M.J., 2003. Characterization of secondary atmospheric photooxidation products: evidence for biogenic and anthropogenic sources. Journal of Geophysical Research-Atmospheres 108.

Stefan, M.I., Bolton, J.R., 1999. Reinvestigation of the acetone degradation mechanism in dilute aqueous solution by the UV/H_2O_2 process. Environmental Science and Technology 30, 870–873.

Stefan, M.I., Hoy, A.R., Bolton, J.R., 1996. Kinetics and mechanism of the degradation and mineralization of acetone in dilute aqueous solution sensitized by the UV photolysis of hydrogen peroxide. Environmental Science and Technology 30, 2382–2390.

Tolocka, M.P., Jang, M., Ginter, J.M., Cox, F.J., Kamens, R.M., Johnston, M.V., 2004. Formation of oligomers in secondary organic aerosol. Environmental Science and Technology 38, 1428–1434.

Volkamer, R., Platt, U., Wirtz, K., 2001. Primary and secondary glyoxal formation from aromatics: experimental evidence for the bicycloalkyl-radical pathway from benzene, toluene, and *p*-xylene. Journal of Physical Chemistry A 105, 7865–7874.

Volkamer, R., Molina, L.T., Molina, M.J., Shirley, T., Brune, W.H., 2005. DOAS measurements of glyoxal as an indicator for fast VOC chemistry in urban air. Geophysical Research Letters 32 Art. No. L08806.

Vollhardt, K.P.C., Schore, N.E., 1994. Organic Chemistry, second ed. W.H. Freeman and Company, New York.

Warneck, P., 1999. The relative importance of various pathways for the oxidation of sulfur dioxide and nitrogen dioxide in sunlit continental fair weather clouds. Physical Chemistry Chemical Physics 1, 5471.

Warneck, P., 2003. In-cloud chemistry opens pathway to the formation of oxalic acid in the marine atmosphere. Atmospheric Environment 37, 2423–2427.

Whipple, E.B., 1970. The structure of glyoxal in water. Journal of the American Chemical Society 92, 7183–7186.

Yu, J.Z., Huang, X.-F., Xu, J., Hu, M., 2005. When aerosol sulfate goes up, so does oxalate: implication for the formation mechanisms of oxalate. Environmental Science and Technology 29, 128–133.

Zhu, L., Nicovich, J.M., et al., 2003. Temperature-dependent kinetics studies of aqueous phase reactions of hydroxyl radicals with dimethylsulfoxide, dimethylsulfone, and methanesulfonate. Aquatic Sciences 65 (4), 425–435.